Facile Postsynthesis of Visible-Light-Sensitive Titanium Dioxide/Mesoporous SBA-15

Zuyuan Wang, Fuxiang Zhang, Yali Yang, Bin Xue, Jie Cui, and Naijia Guan*

Key Lab of Functional Polymer Materials, N&T Joint Academy, Department of Materials Chemistry, College of Chemistry, Nankai University, Tianjin 300071, P. R. China

Received August 29, 2006. Revised Manuscript Received April 12, 2007

Visible-light-sensitive titanium dioxide/mesoporous SBA-15 (TiO_2/SBA-15) composites were synthesized through a postsynthetic approach with the assistance of ethylenediamine. The as-prepared nanocomposites were characterized by XRD, nitrogen adsorption, SEM, HRTEM/EDS, FT-IR, DR UV−vis, and XPS. TiO_2 nanoparticles are homogenously dispersed on the silica SBA-15. XPS analyses indicate that the oxygen atoms of TiO_2 were partially substituted by nitrogen atoms, resulting in good response to the visible-light absorption. Ethylenediamine plays a double role: (1) etching the surface of silica SBA-15 and directing its regeneration and (2) introducing nitrogen atoms to the lattice of TiO_2. The excellent photocatalytic activity of the composites is evaluated via the photodecomposition of phenol in the liquid phase under visible- and ultraviolet-light illumination. The conversion of phenol varies with the content of TiO_2 in the composites, and the optimal value is up to 46.2% under illumination in the visible region.

Introduction

TiO_2 is widely used as an efficient photocatalyst for the removal of organic pollutants in water.[1−4] Compared with other semiconductor materials, TiO_2 exhibits remarkable advantages, such as high photocatalytic efficiency, commercial availability, chemical stability, and environmental friendliness. However, applications of TiO_2 encounter two main obstacles: (1) TiO_2 is active only in the ultraviolet region, because of its wide band gap of 3.0−3.2 eV.[5] Ultraviolet light accounts for less than 5% percent of the solar energy compared to the 45% of visible light. Neither the more intense visible part of the solar spectrum nor interior room lighting can be used with TiO_2 photocatalysts. (2) TiO_2 frequently has a relatively low surface area and pore volume, leading to its low adsorption capacity for some bulk organic pollutants. Ultrafine TiO_2 powders possess high photocatalytic activity, because of their larger specific surface areas and more active sites. However, in this case, high surface energy may lead to a spontaneous agglomeration. Some previous studies have focused on the synthesis of mesoporous TiO_2. Unfortunately, however, in most cases mesoporous TiO_2 is either amorphous or semicrystalline with low photocatalytic activity.[6−8] Thus, new photocatalysts with both high photocatalytic activity when illuminated with visible light and high adsorption capacity must be developed.

Many strategies have been applied to overcome the mentioned shortcomings: (1) Doped TiO_2 has been used widely to extend the useful spectral range into the visible region. Recently, the band gap of TiO_2 was shown to be narrowed by using anionic dopant species.[9,10] Asahi et al. calculated the band structure of nitrogen-doped TiO_2.[11,12] Their results show that substitution of oxygen atoms by nitrogen atoms leads to mixed N 2p and O 2p states and thus to a narrowing of the band gap. Later, many synthetic routes were developed to dope TiO_2 with nonmetal atoms to extend its optical response into the visible region.[13−16] Soft synthesis of doped TiO_2 has been motivated by lowering the reaction temperature; a mild environment allows for the control of the amount and the position of doping elements.[17] (2) Mesoporous materials are considered as an ideal class of catalyst supports because their large surface areas and uniform pore size distribution permit easy diffusion of large organic molecules toward internal active sites. Immobilization of TiO_2 on mesoporous silica may enhance the adsorp-

* To whom correspondence should be addressed. Tel./Fax: +86-22-23500341, E-mail: guannj@nankai.edu.cn.

(1) Dahm, A.; Lucia, L. A. *Ind. Eng. Chem. Res.* **2004**, *43*, 7996.
(2) Li Puma, G.; Khor, J. N.; Brucato, A. *Environ. Sci. Technol.* **2004**, *38*, 3737.
(3) Kutsuma, S.; Toma, M.; Takeuchi, K.; Ibusuki, T. *Environ. Sci. Technol.* **1999**, *33*, 1071.
(4) Lee, D. J.; Senseman, S. A.; Sciumbato, A. S.; Jung, S.-C.; Krutz, L. J. *J. Agric. Food Chem.* **2003**, *51*, 2659.
(5) Yohei, A.; Masakazu, K.; Shu, Y.; Tsugio, S. *J. Solid State Chem.* **2004**, *177*, 3235.
(6) Shiraishi, Y.; Saito, N.; Hirai, T. *J. Am. Chem. Soc.* **2005**, *127*, 12820.
(7) Zhou, Y.; Antonietti, M. *J. Am. Chem. Soc.* **2003**, *125*, 14960.
(8) Zhang, Y.; Li, G.; Wu, Y.; Luo, Y.; Zhang, L. *J. Phys. Chem. B* **2005**, *109*, 5478.
(9) Li, D.; Hajime, H.; Shunichi, H. *Chem. Mater.* **2005**, *17*, 2588.
(10) Zhao, W.; Ma, W.; Chen, C.; Zhao, J.; Shuai, Z. *J. Am. Chem. Soc.* **2004**, *126*, 4782.
(11) Asahi, R.; Morikawa, T.; Ohwaki, T.; Aoki, K.; Taga, Y. *Science* **2001**, *293*, 269.
(12) Morikawa, T.; Asahi, R.; Ohwaki, T.; Taga, Y. PCT WO 01/10553Al, 2001.
(13) Torbjorn, L.; Julius, M. M.; Esteban, A.; Jacob, J.; Anders, H.; Claes-Go1ran, G.; Sten-Eric, L. *J. Phys. Chem. B* **2003**, *107*, 5709.
(14) Shanmugasundaram, S.; Horst, K. *Chem. Phys. Chem.* **2003**, *4*, 487.
(15) Justicia, I.; Ordejon, P.; Canto, G. *Adv. Mater.* **2002**, *14*, 1399.
(16) Hiroshi, I.; Yuka, W.; Kazuhito, H. *J. Phys. Chem. B* **2003**, *107*, 5483.
(17) Shu, Y.; Yohei, A.; Masakazu, K.; Wang, J. S.; Tang, Q.; Tsugio, S. *J. Mater. Chem.* **2005**, *15*, 674.

10.1021/cm062041l CCC: $37.00
Published on Web 05/25/2007

tion and avoid agglomeration.[18−20] Among various mesoporous materials, silica MCM-41 and SBA-15 have been extensively investigated.[21−23] SBA-15 is a mesoporous silica molecular sieve with uniform hexagonal channels ranging from 5 to 30 nm and having framework walls in the thickness range of 3.1−6.4 nm. Because of its thick walls and better hydrothermal stability in comparison with MCM-41, SBA-15 is believed to be a good candidate as supporting matrix of photocatalysts.[23,24]

Direct synthesis and postsynthesis are two main methods for preparation of titanium-coated SBA-15. The procedure of direct synthesis is relatively simple[25−30] and provides a good distribution of titanium species on silica framework surfaces, but the loading by titanium species is always low.[31−33] Compared to direct synthesis, postsynthesis can introduce a higher loading of titanium species on silica SBA-15.[34] However, the postsynthesis routes are usually complicated, and in some cases, the process has to be carried out in the absence of water and oxygen.[35−37] Another disadvantage of postsynthesis is that the uniform mesostructures may be destroyed since titanium species tend to form in the channels or on the external surface of silica SBA-15. These species will have a negative impact on the catalyst performance.[38] So far, supported TiO_2 that is sensitive to visible light has been scarcely reported, because it can hardly be prepared by a simple synthesis route. It is therefore an interesting topic to develop a facile method for the synthesis of TiO_2 materials immobilized on mesoporous silica that can be used as new photocatalysts for practical applications with visible-light illumination.

In this paper, we report a novel and facile amine-assisted postsynthesis for the preparation of TiO_2/SBA-15. TiO_2 nanoparticles are homogeneously dispersed on the silica SBA-15. Furthermore, the as-synthesized composites showed good visible-light response because oxygen atoms of TiO_2 are partly replaced by nitrogen atoms simultaneously. Ethylenediamine plays an important role during the synthetic process. The potential application of these materials as photocatalysts in the visible light is also discussed.

Experimental Section

Materials. Tetraethyl orthosilicate (TEOS, Tianjin Damao Chemical Factory), triblock copolymer poly(ethylene glycol)-*block*-poly(propylene glycol)-*block*-poly(ethylene glycol) (P123, molecular weight = 5800, $EO_{20}PO_{70}EO_{20}$, Nanjing Well Chemical Co.), titanium trichloride ($TiCl_3$,15%, Shanghai Meixing Chemical Company), ethylenediamine (Tianjin 1st Chemical Factory), and HCl were analytically pure and used without further purification. Degussa P-25 TiO_2 (70:30 anatase to rutile, % w/w) with an average particle size of 30 nm and a BET surface area of 55 m^2/g was used as the reference sample.

Synthesis of Mesoporous Silica SBA-15. Mesoporous silica SBA-15 was synthesized according to reported procedures.[39] TEOS and P123 were used as silicon sources and the structure-directing template, respectively. In a typical procedure, 20 g of P123 was dissolved in 600 g of 2 M HCl and 150 g of distilled water with stirring, followed by adding 42.5 g of TEOS at 40 °C. The resulting gel was continuously stirred for 20 h and then crystallized in a Teflon-lined autoclave at 100 °C for 24 h. After crystallization, the solid product was filtered, washed with distilled water, and dried in air at 60 °C for 24 h. The as-synthesized materials were calcined in air at 550 °C for 6 h to remove the organic template, and a white powder (silica SBA-15) was obtained.

Postsynthesis of TiO_2/SBA-15. TiO_2/SBA-15 composites were prepared by an amine-assisted postsynthesis method using $TiCl_3$ as titanium source and ethylenediamine as solvent. In a typical preparation, the desired amount of aqueous $TiCl_3$ and 8 mL of ethylenediamine were mixed. Then 0.5 g of as-synthesized mesoporous silica SBA-15 was added to this mixture. The mixture stirred for 2 h and then placed in a Teflon-lined autoclave at 160 °C for 96 h in a rotating oven for crystallization. After crystallization, the solid product was filtered, washed with distilled water, and dried in air at 60 °C for 24 h. The amount of $TiCl_3$ added varied to give different Ti/Si atomic ratios of 0.02, 0.04, 0.1, and 0.2, and the products were denoted as TNS-1, TNS-2, TNS-3 and TNS-4, respectively.

Control Experiment without Titanium Sources. The as-synthesized silica SBA-15 was directly immersed into 8 mL of ethylenediamine solvent and recrystallized in a Teflon-lined autoclave at 160 °C for 96 h in a rotating oven. After recrystallization, the mixture was filtered, washed with distilled water, and dried in air at 60 °C for 24 h (EDA−SBA-15).

Characterization Methods. The phase composition of the solid products was determined by X-ray diffraction on a Rigaku D/max 2500 diffractometer equipped with graphite-monochromator Cu Kα radiation. Typically, the data were collected from 0.04° to 3.2° with a resolution of 0.02° (small-angle X-ray scattering, SAXS) or between 15° and 60° with a resolution of 0.2° (conventional wide-angle XRD patterns).

Nitrogen adsorption−adsorption isotherms were determined at 77 K using an adsorption porosimeter (TriStar 3000). The surface area measurements were performed according to the BET method.

(18) Li, Y.; Kim, S. J. *J. Phys. Chem. B* **2005**, *109*, 12309.
(19) Tuel, A.; Hubert-Pfalzgraf, L. G. *J. Catal*. **2003**, *217*, 343.
(20) Yang, C.; Chen, C. J. *Appl. Catal. A* **2005**, *294*, 40.
(21) Ettireddy, P. R.; Sun, B.; Panagiotis, G. S. *J. Phys. Chem. B.* **2004**, *108*, 17198.
(22) Han, Y.; Xiao, F.; Wu, S.; Sun, Y.; Meng, X.; Li, D.; Lin, S. *J. Phys. Chem. B* **2001**, *105*, 7963.
(23) Luan, Z.; Larry, K. *Microporous Mesoporous Mater.* **2001**, *44*−*45*, 337.
(24) Luan, Z.; Maes, E. M.; W. van de Heide, P. A.; Zhao, D.; Czemuszewicz, R. S.; Kevan, L. *Chem. Mater.* **1999**, *11*, 3680.
(25) Wu, S.; Han, Y.; Zou, Y.; Song, J.; Zhao, L.; Di, Y.; Liu, S.; Xiao, F. *Chem. Mater.* **2004**, *16*, 486.
(26) Zhang, W.; Lu, J.; Han, B.; Li, M.; Xiu, J.; Ying, P.; Li, C. *Chem. Mater.* **2002**, *14*, 3413.
(27) Bharat, L.; Newalkar, J. O.; Sridhar, K. *Chem. Mater.* **2001**, *13*, 552.
(28) Chen, Y.; Huang, Y.; Xiu, J.; Han, X.; Bao, X. *Appl. Catal. A* **2004**, *273*, 185.
(29) Meng, X.; Li, D.; Yang, X.; Yu, Y.; Wu, S.; Han, Y.; Yang, Q.; Jiang, D.; Xiao, F. *J. Phys. Chem. B* **2003**, *107*, 8972.
(30) Wu, S.; Han, Y.; Zou, Y.; Song, J.; Zhao, L.; Di, Y.; Liu, S.; Xiao, F. *Chem. Mater.* **2004**, *16*, 486.
(31) Vinu, A.; Srinivasu, P.; Niyahara, M.; Ariga, K. *J. Phys. Chem. B* **2006**, *110*, 801.
(32) Wu, P.; Takashi, T. *Chem. Mater.* **2002**, *14*, 1657.
(33) Calleja, G.; Grieken, R.; Garcia, R.; Melero, J. A.; Iglesias, J. *J. Mol. Catal.* **2002**, *182*−*183*, 215.
(34) Landau, M. V.; Vardman, L.; Wang, X.; Titelman, L. *Microporous Mesoporous Mater*. **2005**, *78*, 117.
(35) Luan, Z.; Maes, E. M.; van der Heide, P. A. W.; Zhao, D.; Czernuszewicz, R. S.; Kevan, L. *Chem. Mater.* **1999**, *11*, 3680.
(36) Luan, Z.; Hartmann, M.; Zhao, D.; Zhou, W.; Kevan, L. *Chem. Mater.* **1999**, *11*, 1621.
(37) Luan, Z.; Bae, J. Y.; Kevan, C. *Chem. Mater.* **2000**, *12*, 3202.
(38) Murugavel, R.; Roesky, H. W. *Angew. Chem.* **1997**, *36*, 477.
(39) Zhao, D.; Huo, Q.; Feng, J.; Bradley, F. C.; Galen, D. S. *J. Am. Chem. Soc.* **1998**, *120*, 6024.

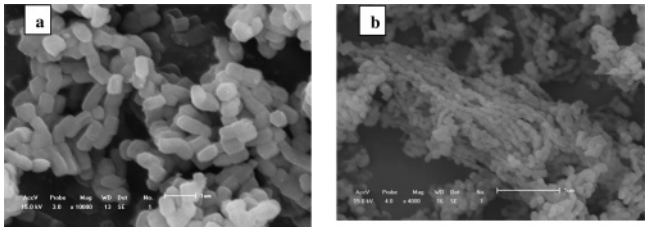

Figure 1. SEM images of (a) original SBA-15 (×4000) and (b) EDA−SBA-15 (×6000).

Pore size distribution was obtained by applying the BJH model. The pore volume was taken at $P/P_0 = 0.974$ (single point).

The particle morphology was analyzed using a transmission electron microscope (TEM JEOL 2010) at an acceleration voltage of 200 kV and a scanning electron microscope (SEM, Shimadzu SS-550) operated at 200 kV. The local Ti/Si ratio was determined by quantitative energy dispersive X-ray analysis (EDS) in STEM mode. An electron beam spot of about 15−25 nm in diameter was used.

Fourier transform infrared (FT-IR) spectra were recorded on a Bruker Vector 22 FT-IR spectrophotometer using a KBr pellet technique. The light absorption of the solid products was performed by diffuse reflectance UV−vis spectra (DR UV−vis). Absorbance spectra were recorded in air against MgO on a JASCO V-550 UV−vis spectrophotometer. The X-ray photoelectron spectroscopy (XPS) measurements were acquired using a PHI 5300 ESCA XPS spectrometer with monochromatic Mg Kα excitation, and all the bonding energies were calibrated to the C 1s peak at 284.6 eV of the surface adventitious carbon.

Photocatalytic Tests. The photocatalytic activity of sample powders was evaluated in a three-phase fluid bed photoreactor (Golden Eagle Technology Co., Ltd.), equipped with ultrahigh-pressure mercury lamps (100 W, >420 nm and 120 W, >360 nm). For experiments under visible light, 220 mL of an aqueous phenol solution at a concentration of 40 mg/L and containing 0.5 g of catalyst were loaded in this quartz photoreactor. The temperature of the photoreactor was kept at 25 °C using a recycling cooling water system. The aqueous solutions were forced to recycle in the pipelines with 15 L/h flow rate by a liquid pump, and the gas atmosphere was bubbled by a mini gas pump through the gas distributor. Finally, the total organic carbon (TOC) was also measured using a Shimadzu TOC-V CSH analyzer to evaluate the photomineralization degree.

Results and Discussion

Etching and Regrowth of EDA−SBA-15. Generally, original SBA-15 particles have the shape of curved cylinders. Their typical diameter is 200−400 nm and their length is 1−2 μm. An aggregation between particles can be easily found in our SEM observations (see SEM images in Figure 1a). The EDA−SBA-15 particulates typically formed hexagonal disks smaller than the original SBA-15 and were coalesced into chainlike arrays, as demonstrated in Figure 1b. The post-treated products have the unique morphology of bundles. The bundles are composed of long, thin, chainlike structures fused together.

Figure 2 shows the small-angle XRD patterns of pure silica SBA-15 and EDA−SBA-15. The three well-resolved peaks can be indexed as (100), (110), and (200) reflections associated with hexagonal space group *P6mm*, suggesting a well-ordered mesostructure. After the treatment, the intensity of the (100) reflection became weaker while the (110) reflection remained unchanged. The TEM image in Figure 3 shows the coalesced part of two individual silica SBA-15 particles. They indicate the high structural order of parallel nanochannels having a uniform diameter. In the coalesced part, the silica SBA-15 particles are connected through the reconstruction of curved nanochannels along the (110) direction.

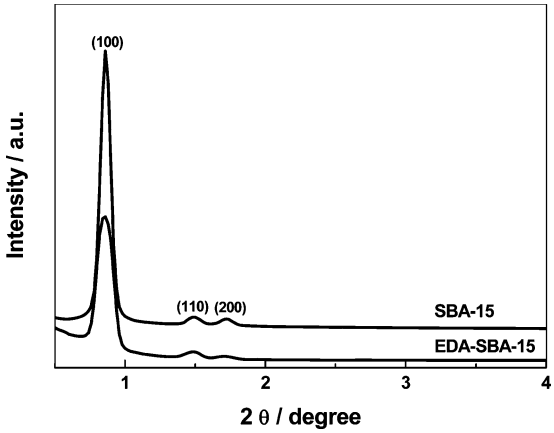

Figure 2. Small-angle XRD patterns of SBA-15 and EDA−SBA-15.

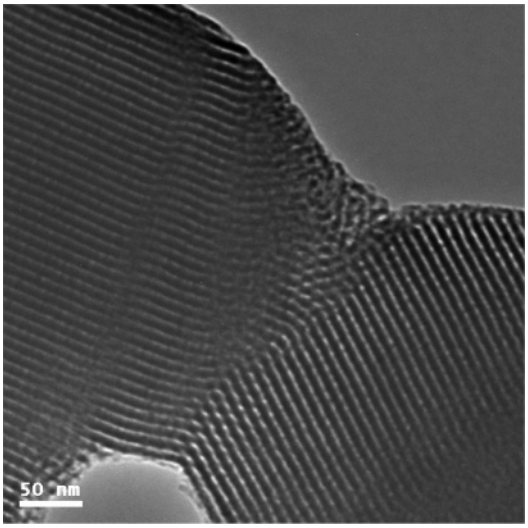

Figure 3. TEM image of EDA−SBA-15 viewed along the (110) direction.

Table 1. Textural Properties of the As-Synthesized Materials

sample	pore diameter (nm)	surface area (m^2/g)	pore volume (cm^3/g)	bandgap (eV)
SBA-15	8.02	741.9	1.04	
EDA−SBA-15	10.76	406.9	1.02	
TNS-1	9.68	389.1	0.69	2.92
TNS-2	9.51	331.8	0.56	2.43
TNS-3	9.14	236.7	0.27	1.98
TNS-4	6.93	197.4	0.21	1.95

The silica SBA-15 has a BJH pore size of 8.02 nm and a surface area of 742 m^2/g calculated by the BET method (see Table 1). The EDA−SBA-15 has an obviously larger pore size of 10.76 nm and a lower surface area of 407 m^2/g. Therefore, it can be seen that the pore wall of silica SBA-15 is partly dissolved by the post-treatment under alkaline conditions. The regenerated silica SBA-15 is packed and distorted to jam the pore channels, which results in the decrease of the surface areas.

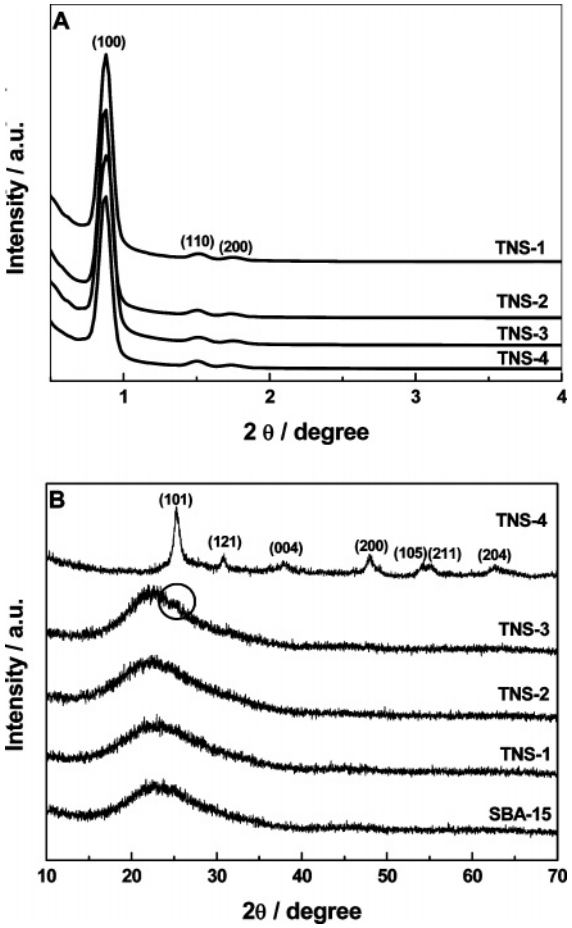

Figure 4. (A) Small-angle XRD patterns of postsynthetic samples. (B) Wide-angle XRD patterns of pure silica SBA-15 and postsynthetic samples.

During the treatment, ethylenediamine plays a double role. The adsorption of ethylenediamine on the (100) plane of silica SBA-15 results in a slow chemical etching under alkaline conditions at increasing temperature. On the other hand, serving as a structural orienting agent, ethylenediamine also promotes the regrowth of the (100) plane of silica SBA-15. During the chemical etching process, the exposed hydroxyls on the surface of the individual segments tended to condense, leading to dehydroxylation. This process contributes to control the morphology and enables the creation of active sites in SBA-15.

Characterization of TiO_2/SBA-15. Figure 4 shows XRD patterns of pure silica SBA-15 and four postsynthetic samples, TNS-1, TNS-2, TNS-3, and TNS-4. Figure 4A shows the results obtained at lower scattering angle region. The three well-resolved peaks could be indexed as (100), (110), and (200) reflections associated with hexagonal space group *P6mm*.[40] As the molar ratio of Ti/Si decreases, the intensity of the (100) reflection became weaker while the (110) and (200) reflections remained unchanged.

Figure 4B shows the XRD results obtained in the wide-angle region. As no distinguishable peak was found, the as-synthesized pure silica SBA-15 is amorphous. For the TNS-1 and TNS-2 samples with lower Ti/Si ratio, a broad diffraction peak centered at about 23° also was detected. The lack of

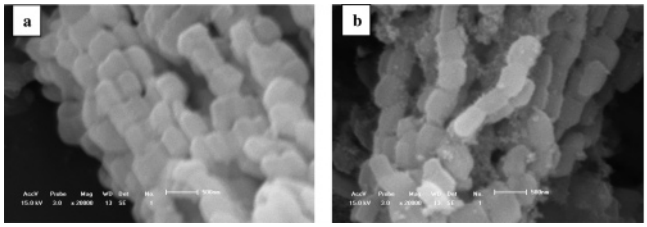

Figure 5. SEM images of as-synthesized samples (a) TNS-1 and (b) TNS-4.

specific diffraction lines of crystalline TiO_2 indicates that TiO_2 existed either as particles smaller than 3 nm or that the characteristic peaks of TiO_2 were muffled by the diffraction peak of the SiO_2 amorphous phase. With increasing Ti/Si ratio to 0.1, the faint peak of the (101) reflection for TiO_2 could be detected in TNS-3 (see Figure 4B), indicating that the anatase phase emerged and became distinct. Furthermore, the peaks in TNS-4 corresponding to reflections of the (101), (004), (200), (105), (211), and (204) planes are assigned to the anatase phase of TiO_2 and the reflection of the (121) plane to the brookite phase, while reflections of the rutile phase are absent.[34] The results clearly indicate that increasing the amount of titanium precursors in the synthesis gels facilitated the formation of extraframework TiO_2.

The specific surface areas (BET) and the pore sizes of these samples were calculated by the BJH method, and the results are summarized in Table 1. The pore size of the TiO_2/SBA-15 samples is slightly larger than that of silica SBA-15, except for sample TNS-4. The latter result is attributed to the aggregated TiO_2 nanoparticles formed on the external surface of SBA-15. With increasing Ti/Si ratio, the pore volume dropped from 0.69 to 0.21 cm^3/g and the surface area decreased from 407 to 197 m^2/g. These results suggest that a high density of TiO_2 nanoparticles had been loaded on the SBA-15 support.

Figure 5 shows the SEM images of TNS-1 and TNS-4. The morphology of the individual silica SBA-15 samples does seem to be strongly changed after amine-assisted postsynthesis. Each SBA-15 was self-assembled one by one in a ropelike pattern.[41] TiO_2 should be homogenously distributed on the surface of SBA-15 in the case of the low Ti/Si ratio. With increasing titanium loading, some TiO_2 crystallites are observed on the external surface of silica SBA-15 (see Figure 5b).

The homogeneity of the distribution of titanium and its influence on the well-ordered hexagonal array of silica SBA-15 were further studied by high-resolution transmission electron microscopy (HRTEM). The pore diameters of the mesoporous pure silica SBA-15 are about 5−7 nm, with well-defined arrays of nanochannels (see Figure 6a). It is still surprising to find that the individual silica SBA-15 is self-assembled in ethylenediamine in the (100) plane direction, which is propitious to the incorporation of TiO_2. As shown in Figure 6b,c, along the (110) direction, there is a regular hexagonal array of uniform channels characteristic of mesoporous SBA-15. The introduction of titanium species, therefore, does not alter the ordered array of mesopores. TiO_2

(40) Zile, H.; Bu, W.; Lian, Y.; Chen, H.; Li, L.; Zhang, L.; Li, C.; Shi, J. *J. Mater. Chem.* **2005**, *15*, 661.

(41) Zhao, D.; Sun, J.; Li, Q.; Stucky, G. D. *Chem. Mater.* **2000**, *12*, 275.

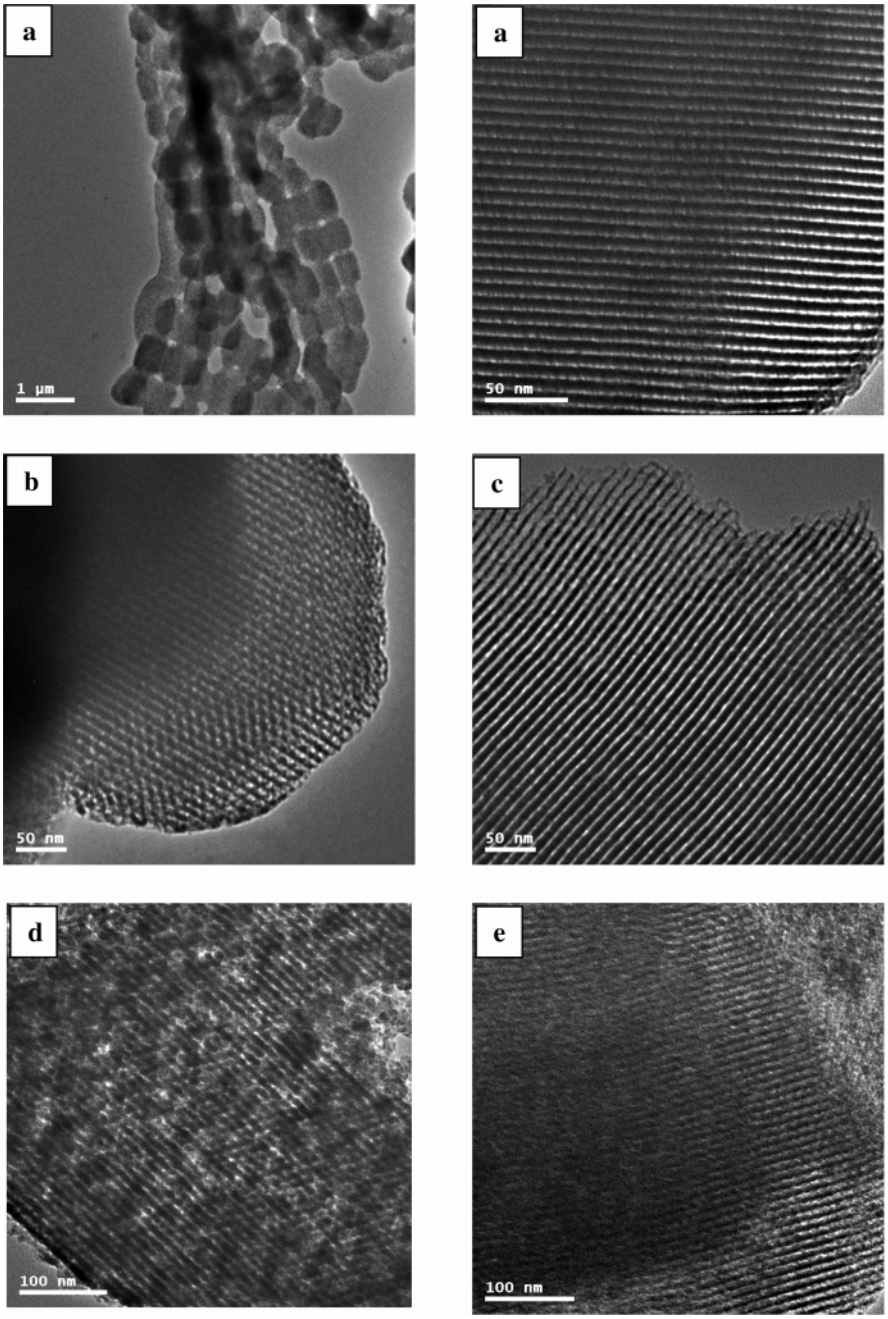

Figure 6. HRTEM images of (a) pure silica SBA-15, (b) TNS-1, (c) TNS-2, (d) TNS-3, and (e) TNS-4.

nanoparticles were not found obviously in Figure 6b,c, indicating the homogeneous distribution of TiO_2 in samples with low Ti/Si ratio, consistent with the results of the XRD patterns. However, as shown in Figure 6d,e, with the increasing titanium loading, some TiO_2 crystallites emerged on the external surface of SBA-15 with the particle size increased, possibly due to aggregation of semiconductor particles.

The HRTEM images of as-synthesized TNS-1 in Figure 7show that a series of necklace-like SBA-15 were formed with well-dispersed titanium species. The channel diameter was intact compared to that of the parent SBA-15 in spite of a decrease of the region with lower silica density due to titanium species incorporation. Direct evidence of the formation of TiO_2 within mesoporous silica SBA-15 (Figure 7) can be obtained from the qualitative energy dispersive spectrum of TEM, which exhibits the characteristic peaks of Ti [0.52 keV (Ka) and 4.93 keV (Kb)] and of Si [1.74 keV (Ka)].[42] The Ti/Si atomic ratio is calculated to be 0.019. On the basis of these results, we can conclude that the Ti peak comes from the core part (TiO_2) and the Si peak is contributed from the silica in the SBA-15 supporting materials.

FT-IR spectroscopy is a useful technique for characterizing the framework titanium species in mesoporous crystalline SBA-15. Figure 8 shows FT-IR spectra of pure silica SBA-15 and TiO_2/SBA-15 with various Ti/Si molar ratios. In all the spectra, the broad bands at about 3437 and 1636 cm^{-1} attributed to the stretching vibration of hydroxyl groups and water and to the deformation vibration of water can be

(42) Ok, K. P.; Young, S. K. *Colloids Surf. A* **2005**, *257*−*258*, 261.

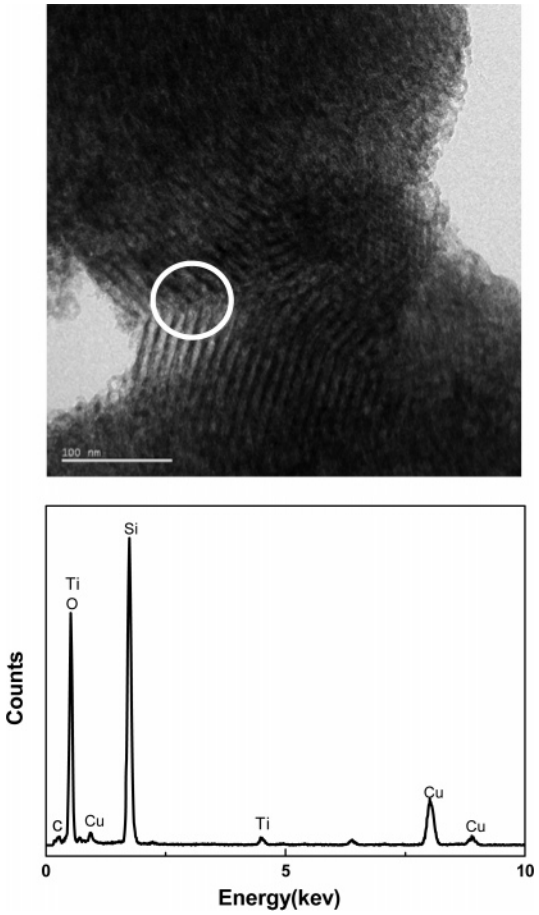

Figure 7. HRTEM/EDS spectra of the sample TNS-1.

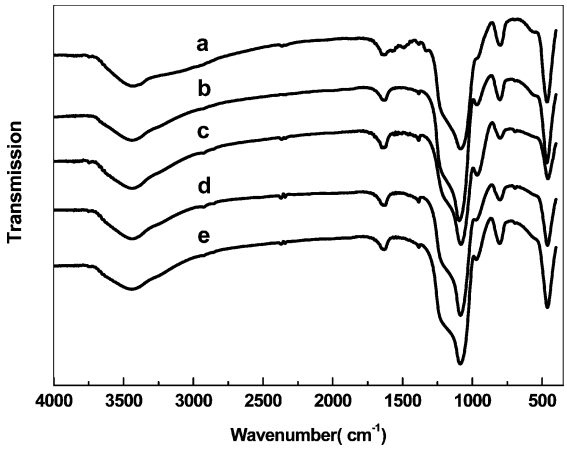

Figure 8. FT-IR transmission spectra in the 4000−470 cm^{-1} region of (a) pure silica SBA-15, (b) TNS-1, (c) TNS-2, (d) TNS-3, and (e) TNS-4.

observed, respectively. The presence of molecular water is most likely connected with the KBr. The peak at 1104 cm^{-1} corresponds to the asymmetric stretching vibration of Si−O−Si and the bands at 800 and 470 cm^{-1} can be assigned to the symmetric stretching and deformation modes of Si−O−Si. Theoretically, the IR band observed at 910−960 cm^{-1} might be assigned to the Ti−O−Si stretching vibration. Additionally, the band at 960 cm^{-1} is conventionally a fingerprint of the existence of Si−O−Ti bonds and its enhancement correlates with the titanium species anchored on the surface of silica SBA-15.[43] For the parent silica SBA-15, this peak was attributed to the Si−OH stretching vibration. However, the peak intensity of TiO_2/SBA-15 was a little higher than that of parent SBA-15 when increasing the Ti/Si ratio.

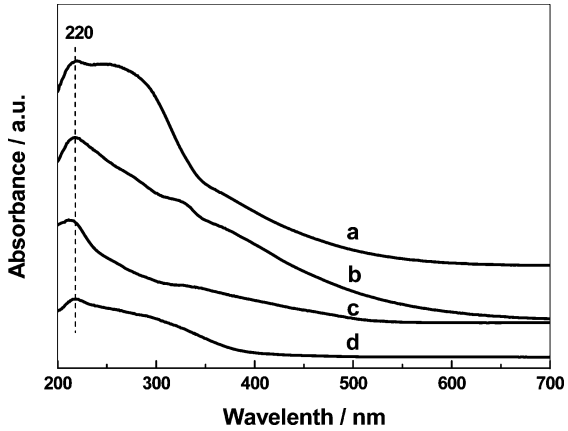

Figure 9. UV−vis spectra of the as-synthesized samples (a) TNS-4, (b) TNS-3, (c) TNS-2, and (d) TNS-1.

Visible-light sensitivity is indicated by the DR UV−vis spectra in Figure 9 and the band gap energy of the samples as shown in Table 1. The DR UV−vis spectra of the samples exhibit two characteristic absorption bands: namely, an absorption band centered at 220 nm and a broad signal around 300−350 nm. The bands increase clearly upon increasing of titanium loading on the silica surface of the mesoporous material, which corresponds to the presence of extraframework titanium species. The chain-type Ti−O−Si−O−Ti structures could be attributed the band at 220 nm, which indicates the interaction of titanium species and the surface of supports. The broad absorption band around 300−350 nm originates from the band gap energy of bulk titania.[44] Thus, the strong peak around 300−350 nm in Figure 9 suggests that the addition of SBA-15 can effectively suppress the growth of TiO_2 particles. These spectroscopic results confirm that titanium species are located in the framework of SBA-15 and are partially dispersed as TiO_2 on the particle surface at a high titanium loading. The DR UV−vis spectra of TiO_2/SBA-15 have a new peak in the region 400−500 nm compared with that of silica SBA-15. In previous studies of nitrogen-doped TiO_2, a distinctive peak at 400−500 nm is attributed to the substitution of oxygen atoms with nitrogen atoms.[13−16] Thus we believe that the nitrogen atoms have been incorporated into the TiO_2 crystalline structure, which is the origin of the visible-light response, because partial doping of nitrogen atoms can induce the generation of a new state lying close to the valence band edge.

The presence of incorporated nitrogen in TiO_2/SBA-15 could also be demonstrated by XPS (see Figure 10). The N 1s peak (Figure 10 b) was observed near 400 eV for TNS-4 but was detectable neither for TNS-1 nor for pure SBA-15. Asahi et al. reported the N 1s XPS peak of O−Ti−N at 396 eV.[11] There were several other reports concerned with XPS investigations and the enhanced photocatalytic activity of the

(43) Natalia, N. T.; Alexander, A. P.; Emil, R. *Langmuir* **2005**, *21*, 10545.

(44) Chiker, F.; Launay, F.; Nogier, J. P.; Bonardet, J. L. *Green Chem.* **2003**, *5*, 318.

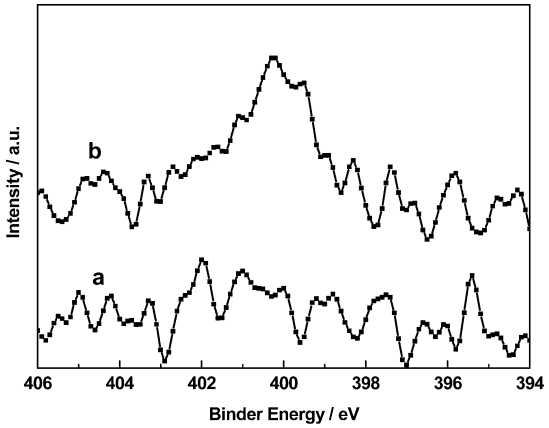

Figure 10. XPS spectra of the as-synthesized samples (a) TNS-1 and (b) TNS-4.

nitrogen-containing systems.[45,46] In these reports, the N peak at 396 eV was not always observed while a nitrogen peak around 404 eV could be detected, even if the noise was very high.[47] Chen et al. explained that the signal at 401.3 eV was attributed to O−Ti−N, based on the redox chemistry involved and the XPS peak positions of oxygen and titanium.[48] Thus, the N 1s binding energy of Ti−N may vary from case to case. For TNS-4, the signal at 400.3 eV is believed to characterize the nitrogen in O−Ti−N. On the basis of this result, we infer that in our TiO_2 system nitrogen atoms are incorporated into the TiO_2 lattice as O−Ti−N species. Therefore, the $TiO_{2-x}N_x$ appears more easily on the extraframework TiO_2 or the surface of SBA-15 with high molar ratio of Ti/Si.

Mechanism of TiO_2 Grafting and Nitrogen Substitution. By means of the novel postsynthesis, ethylenediamine induced both a partial reconstruction of silica SBA-15 and the formation of Ti−O−Si bonds simultaneously. It is known that ethylenediamine is an excellent solvent for solvothermal syntheses. The critical pressure of ethylenediamine is 62.1 atm, lower than that of water. Such a relatively low critical pressure makes it possible to carry out many reactions at mild temperature.[49] We propose that dissolution and regrowth of SBA-15 mesoporous molecular sieve occur. With the increasing temperature, the preadsorbed ethylenediamine selectively etched the surface on the (100) plane of silica SBA-15. Ethylenediamine served as a structure-orienting agent and promoted the growth of plane (100) for silica SBA-15. Simultaneously, $TiCl_3$ was slowly hydrolyzed in the ethylenediamine solvent.[17] During the chemical etching process, the exposed hydroxyls on the surface of SBA-15 and from titanium species tended to condense.[27] Therefore, titanium species were well-distributed on the surface and anchored onto the surface of silica SBA-15 during the particular postsynthesis. The presence of ethylenediamine facilitated the grafting of TiO_2 onto the surface of SBA-15.

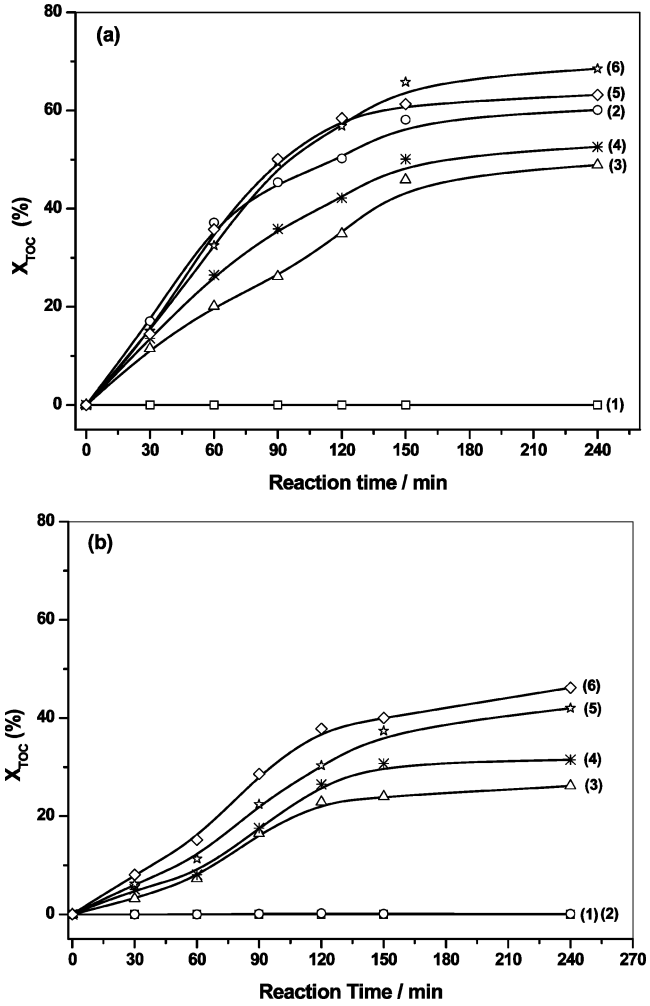

Figure 11. Photocatalytic degradation of phenol under ultraviolet-light illumination (a) and visible-light illumination (b) on different catalysts: (1) blank, (2) P-25 TiO_2, (3) TNS-1, (4) TNS-2, (5) TNS-3, and (6) TNS-4. Experimental conditions: 0.5 g of catalyst, 25 °C, flow rate 15 L/h.

From the viewpoint of nitrogen doping, previous researchers reported that the synthesis of TiO_2 from $TiCl_3$ in the presence of organic amines creates new absorption bands in the visible spectra.[5,17] Nitrogen doping of TiO_2 induced visible-light sensitivity in the presence of ethylenediamine, as reported previously.[50] The characterizations reported in the present paper further verified the nitrogen doping in our systems. FT-IR spectra in Figure 8 reveal that ethylenediamine is not present in the samples as expected. XRD patterns in Figure 4 rule out the existence of crystalline TiN materials. The DR UV−vis spectra (Figure 9) show the presence of a new peak in the region 400−500 nm, which is induced by the substitution of oxygen atoms by nitrogen atoms in TiO_2. Furthermore, the signal at 400.3 eV in XPS spectra is attributed to the N 1s binding energy in the Ti−N linkage.

Each nitrogen atom of ethylenediamine offers a pair of electrons so that each is capable of forming a coordinate covalent bond with metal ions. In this paper, $TiCl_3$ and ethylenediamine combine as a bidentate ligand intermediate

(45) Sano, T.; Negishi, N.; Koike, K.; Takeuchi, K.; Matsuzawa, S. *J. Mater. Chem.* **2004**, *14*, 380.
(46) Diwald, O.; Thompson, T. L.; Goralski, E. G.; Walck, S. D.; Yates, J. T., Jr. *J. Phys. Chem. B* **2004**, *108*, 52.
(47) Sakthivel, S.; Kisch, H. *ChemPhysChem.* **2003**, *4*, 487.
(48) Chen, X.; Clemens, B. *J. Phys. Chem. B* **2004**, *108*, 15446.
(49) Xu, Y.; Masaru, O.; Tatsuya, O. *Microporous Mesoporous Mater*. **2004**, *70*, 1.
(50) Wang, Z.; Zhang, F.; Yang, Y.; Cui, J.; Sun, Q.; Guan, N. *Chin. J. Catal.* **2006**, *27*, 1091.

to form relatively stable Ti^{3+} complexes. The solvothermal system contributes the positive effect of Ti←N ligand-to-metal charge transfer.[51] The transformation of Ti^{3+} to Ti^{4+} results in an oxygen vacancy, providing nitrogen atoms more opportunities to occupy the sites of oxygen atoms in the growing crystal. This indirectly reveals larger amounts of nitrogen atoms incorporated into the TiO_2 lattice; however, the origin of the nitrogen doping remains unclear.

Photocatalytic Activity. Phenol, an aromatic pollutant, was employed to evaluate the photocatalytic activity of the as-synthetic composites under ultraviolet and visible-light illumination. The TOC removal ratio was calculated as follows:

$$X_{TOC} = ([TOC]_0 - [TOC]_t)/[TOC]_0$$

where X represents the percentage conversion, $[TOC]_0$ is the concentration at initial time, while $[TOC]_t$ is the concentration at any other time. It was demonstrated from the TOC data shown in Figure 11 that the phenol degradation ratio on the as-synthesized samples increased with the increase of TiO_2 content under the irradiation of both ultraviolet and visible light. The optimal photocatalytic performances were observed on the TNS-4 sample with X_{TOC} values of 63.2% and 46.2% after 240 min of ultraviolet and visible-light irradiation, respectively. It is worthy of being mentioned that the ultraviolet activities of samples TNS-3 and TNS-4 are superior to that (60.1%) of the commercial Degussa P-25 TiO_2 catalyst (Figure 11a). One reasonable explanation to the better photocatalytic activity should include the following: (i) nitrogen doping narrowed the band gap of TiO_2, improving the visible-light absorption; (ii) the high specific surface areas of the supports facilitated the mass transfer of reactants and products; (iii) the well-dispersed titanium species provide more active sites for phenol degradation. As an additional illustration, pure silica SBA-15 showed no obvious photocatalytic degradation of aqueous phenol under the irradiation of visible light, and pure P-25 TiO_2 exhibited no phenol conversion due to its limitation of visible-light absorption (Figure 11b).

(51) Akvario, M.; Carbonell, E.; Fornés, V.; García, H. *ChemPhysChem.* **2006**, *7*, 200.

Conclusions

In summary, visible-light-sensitive TiO_2/SBA-15 materials were first synthesized through a novel amine-assisted route. TiO_2 nanoparticles are homogeneously dispersed on the silica SBA-15. XPS analyses indicate that oxygen atoms of TiO_2 were partially substituted by nitrogen atoms, resulting in good response to the visible-light absorption. Ethylenediamine plays a double role in the synthetic process: (1) etching the surface of silica SBA-15 and directing its regeneration and (2) introducing nitrogen atoms into the lattice of TiO_2. The materials exhibit excellent photocatalytic activity for the removal of phenol under both visible- and ultraviolet-light illumination. It is therefore expected that the visible-light-sensitive TiO_2/SBA-15 composites may be a promising liquid-phase oxidation catalyst for practical application.

Acknowledgment. This research was financially supported by National Basic Research Program of China (also called 973, Grant No. 2003CB615801) and National Natural Science Foundation of China (Grant Nos. 20233030, 20573059, and 20603019).

CM062041L